Article ID: 1007-7294(2024)12-1864-16

Numerical Investigation on Hydrodynamic Characteristics of a Tunneled Planing Hull in Calm Water

WANG Hui[1,2], *ZHU Ren-chuan*[1], *LI Guo-huan*[3], *XU De-kang*[1], *LI Chao-fan*[1]

(1. State Key Laboratory of Ocean Engineering, School of Naval Architecture, Ocean and Civil Engineering, Shanghai Jiao Tong University, Shanghai 200240, China; 2. Wuhan Second Ship Design and Research Institute, Wuhan 430205, China; 3. Guangzhou Marine Engineering Corporation, Guangzhou 510250, China)

Abstract: A tunneled planing hull has unique hybrid hydrodynamic and aerodynamic characteristics due to the presence of a tunnel. In this paper, experimental and numerical investigations on hydrodynamic analysis of a tunneled planing hull are carried out. The resistance tests of models with three different masses (127.4 kg, 159.5 kg, 202.9 kg) are conducted for the Froude number in the range of $0.761 \leqslant Fn \leqslant 1.925$. The results of resistance measured by towing tank imply that the tunneled planing hull with a larger displacement has a superior resistance performance. The numerical simulation of Reynolds Average Navier Stokes (RANS) equations based on the finite volume method is performed to analyze the hull characteristics in calm water (M=159.5 kg) with two degrees of freedom (sinkage and trim). The numerical results are compared with the experimental data, which shows good agreement. Pressure distribution, wave profiles and lift forces obtained by SST $k-\omega$ and Realizable $k-\varepsilon$ turbulence models are compared and discussed. Finally, the local fluid flow of streamline around the hull can be divided into four regions due to the presence of a tunnel, which is different from the behaviors of the conventional planing monohull with prismatic form.

Key words: tunneled planing hull; experimental test; overset mesh method; pressure distribution; lift force

CLC number: U661.31 **Document code:** A **doi:** 10.3969/j.issn.1007-7294.2024.12.005

0 Introduction

High-speed planing hulls are widely used for racing and the military due to their high speed and exceptional resistance performance[1]. Various strategies have been used to increase the speed and improve performance, such as chine, step, strake, pad and tunnels[2]. Tunneled planing hulls can create both aerodynamic and hydrodynamic forces to lift the hulls and reduce the wetted areas at high speed, which mainly accounts for the significant resistance reduction[3].

Until now, there are extensive studies on the hydrodynamic analysis of high-speed planing hulls in calm water[4-10]. Generally, the towing tank experimental tests are still the important way to evaluate the performance of high-speed planing hulls. Su et al[11] studied the hydrodynamic perfor-

Received date: 2024-06-13

Foundation item: Supported by the YEQISUN Joint Funds of the National Natural Science Foundation of China (U2141228)

Biography: WANG Hui(1994-), male, Ph.D. candidate;

ZHU Ren-chuan(1969-), male, professor, corresponding author, E-mail: renchuan@sjtu.edu.cn.

mance of a channel-type planing trimaran. A series of hydrodynamic experiments in the towing tank were carried out and the results of experiments revealed the hydrodynamic characteristics of channel type planing hull at high forward speed.

Considering that the experimental model is expensive financially and time-consuming, there are certain limitations in the model tests. With the advancement in computer hardware and software, computational fluid dynamics (CFD) methods are rapidly gaining popularity for the simulation of planing hulls in the last decade. Yousefi et al [12] reviewed a comprehensive study on the existing techniques for analysis and numerous investigations of planing hulls over the past several decades. The finite volume method (FVM) was considered as more appropriate and capable of solving complex free-surface flows around planing hulls in their study. Ghassabzadeh and Ghassemi[13] carried out the numerical simulation with a dynamic mesh restructuring method to determine the hydrodynamic forces on the multi-hull tunnel vessel in a steady motion. They used the non-uniform rational B-Spline method to generate the tunnel hull form. The numerical results in comparison with towing test resistance for a four-tunnel vessel model showed that the proposed numerical algorithm in their study is a promising method for investigation of wide-ranging high-speed vessel types, particularly tunnel vessels[13]. Jiang et al[14] obtained the results of experimental and numerical studies on the planing trimaran hull and analyzed the tunnel hydrodynamic characteristics. They adopted a CFD code based on the finite volume method to simulate the motion of the hull body. The numerical results were compared with measured data and showed good agreement. They also investigated the influence of tunnel configuration on the hydrodynamic behaviors of planing trimarans. They found that the tunnel lift has a direct influence on the resistance performance. Then, the hybrid hydrodynamic and aerodynamic performance due to the presence of a tunnel were studied[15]. Numerical results implied that the aerodynamic forces provide major tunnel lift for the speeds higher than Froude number of 4.52. Roshan et al[16] used commercial software Star-CCM+ to simulate a tunneled planing hull in calm water. They discussed various physical phenomena around the hull and introduced a new parameter, i.e. tunneled efficiency. Ding and Jiang presented a detailed numerical investigation of a high-speed planing trimaran to study the tunnel flow mechanism and its effects on resistance. They concluded that the tunnel can absorb the internal wave energy to generate additional lift force. The maximum tunnel aerodynamic lift supports no more than 3% of total displacement and hydrodynamic lift is still dominant in the tunnel lift for planing trimaran.

According to the above literatures, a tunneled planing hull has unique hydrodynamics due to its tunnel. However, the comprehensive hydrodynamic evaluation of tunneled planing hulls by experimental and numerical investigations has rarely been carried out. Therefore, in the current paper, the details of the hydrodynamic performance of a tunneled planing hull at different speeds in calm water will be studied and discussed using experimental tests and numerical simulation. Considering the capacity in the numerical simulation of viscous flow with the complex free surface[15], CFD simulations using two different turbulent models including SST $k-\omega$ and Realizable $k-\varepsilon$ turbulence models will be conducted and compared to investigate the tunnel flow and characteristics of the tunneled planing hull in calm water.

1 Model test

1.1 Physical description of tunneled planing hull

The geometry and configuration of a tunneled planing hull are shown in Fig.1 and the main parameters of the hull are presented in Tab.1. The scale ratio of this model is 1:4. It can be seen that the tunnel starts stem and extends aft to the transom stern. At the bottom of the planing hull, the mid-longitudinal plane is a symmetrical and longitudinally penetrating tunnel, which divides the bottom into three planing surfaces, namely the tunneled planing surface and two side-bottom planing surfaces (see Fig.1). The hydrodynamic and aerodynamic lift force generated by the tunnel and two demihulls support the weight of the hull during the forward motion. The spray and bow waves generated by the hull are absorbed by the large inlet of the tunnel. The water and air in the tunnel are compressed due to the reduction of the space[11]. Model tests of the tunneled planing hull in calm water were conducted in the towing tank of China Special Vehicle Research Institute (No.605 Research Institute).

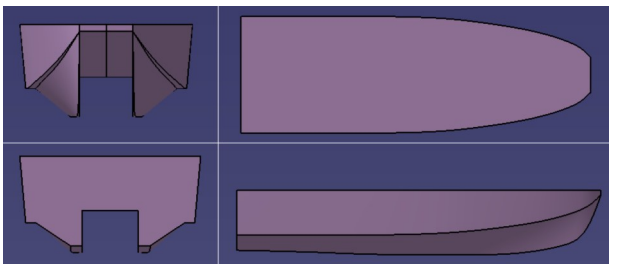

Fig.1 Geometry of the tunneled planing hull

Tab.1 Main parameters of tunneled planing hull

Parameter	Symbol	Value
Length overall /m	L	2.625
Beam /m	B	1.0
Draft /m	D	0.217
Mass /kg	M	127.4, 159.5, 202.9
Longitudinal center of gravity /m	LCG	1.05
Vertical center of gravity /m	VCG	0.325

1.2 Experimental results

The results of calm water resistance tests are summarized in Fig.2. The non-dimensional sinkage is defined as the ratio of sinkage to static draft and the non-dimensional resistance is defined as the ratio of resistance to the weight, respectively. And all the values are plotted against the length Froude number (Fn). In this paper, the length Froude number Fn is used and defined as:

$$Fn = \frac{U}{\sqrt{gL}} \tag{1}$$

where, U is the speed of the vessel, L denotes the length overall and g=9.81 m/s^2 is the gravitational constant.

As shown in Fig.2(a), the non-dimensional sinkage increases with the increasing mass. At the lower speed (Fn=0.761), the hull operates in the semi-planing region, and the hydrodynamic force acting on the bottom causes a trim angle. After the Froude number is over 1.267, the sinkage increases slightly with the increase of speeds. The trim angle increases by increasing the mass in the

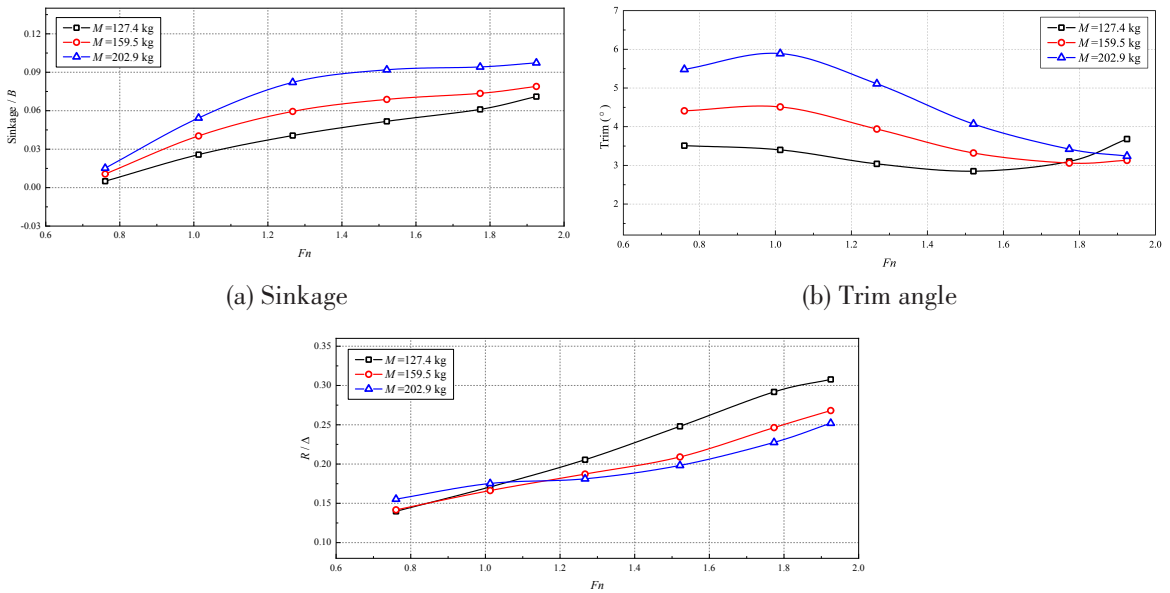

(a) Sinkage　(b) Trim angle

(c) Resistance

Fig.2 Experimental results of three different masses

range of 0.761≤*Fn*≤1.773. With the reduction of the massamount, the craft comes up more from the water. And then the longitudinal center of the pressure moves to the vessel stern and it becomes closer to the center of the mass. In this situation, the trim angle is reduced due to the decrease of the trim moment. The trim angle goes up to a maximum and then decreases gradually with the speed increases. At the higher speed (*Fn*=1.925), the trim angle becomes a relatively steady value. At the lower speed (*Fn*≤1.013), the resistance to lift ratio (*R*/Δ) of *M*=202.9 kg is larger than those of the other two conditions. However, with the increment of the mass, the resistance to lift ratio (*R*/Δ) decreases obviously at high towing speed (*Fn*≥1.267). This behavior of resistance of the tunneled planing hull is consistent with those of the previous studies, which implies that the tunneled planing hull has a superior resistance performance with a larger displacement.

2 Numerical methodology

2.1 Numerical setup

The flow around the planing hull is complex and the governing equations are the continuity equation and incompressible Navier–Stokes equations[17]. In this study, the planing hull was assumed to be a rigid body, and the deformation of the craft was omitted. The unsteady Reynolds Averaged Navier Stokes (RANS) equations were solved using the finite volume method (FVM) based on an implicit and iterative solver in this study. In this paper, two different turbulent models including the SST $k-\omega$ turbulence model and the Realizable $k-\varepsilon$ turbulence model were used to investigate the hydrodynamics of the tunneled planing hull in calm water (*M*=159.5 kg). SST $k-\omega$ turbulence model of transport equation is as follows:

$$\begin{cases} \dfrac{\partial}{\partial t}(\rho k)+\dfrac{\partial}{\partial x_i}(\rho k\bar{u}_i)=\dfrac{\partial}{\partial x_j}\left(\Gamma_k\dfrac{\partial k}{\partial x_j}\right)+G_k-Y_k \\ \dfrac{\partial}{\partial t}(\rho\omega)+\dfrac{\partial}{\partial x_i}(\rho\omega\bar{u}_i)=\dfrac{\partial}{\partial x_j}\left(\Gamma_\omega\dfrac{\partial\omega}{\partial x_j}\right)+G_w-Y_w+S_w \end{cases} \quad (i=1,2,3) \tag{2}$$

where, k denotes the turbulent kinetic energy and ω denotes the dissipation rate. Γ_k, Γ_w, G_k, G_w, Y_k, Y_w and S_w denote the production, dissipation, and cross-diffusion term of k and ω, respectively.

Another CFD model was established by solving RANS equations with Realizable $k-\varepsilon$ turbulence model. The Realizable $k-\varepsilon$ model was employed due to its high numerical stability and accuracy for the pressure gradient solution. The transport equations of turbulent energy and dissipation rate are written as follows:

$$\begin{cases} \rho\dfrac{\mathrm{d}k}{\mathrm{d}t}=\dfrac{\partial}{\partial x_i}\left[\left(\mu+\dfrac{\mu_\mathrm{t}}{\sigma_k}\right)\dfrac{\partial k}{\partial x_i}\right]+G_k+G_\mathrm{b}-\rho\varepsilon-Y_M \\ \rho\dfrac{\mathrm{d}\varepsilon}{\mathrm{d}t}=\dfrac{\partial}{\partial x_i}\left[\left(\mu+\dfrac{\mu_\mathrm{t}}{\sigma_\varepsilon}\right)\dfrac{\partial\varepsilon}{\partial x_i}\right]+\rho C_1S\varepsilon-\rho C_2\dfrac{\varepsilon^2}{k+\sqrt{\nu\varepsilon}}+C_{1\varepsilon}\dfrac{\varepsilon}{k}C_{3\varepsilon}G_\mathrm{b} \end{cases} \quad (i=1,2,3) \tag{3}$$

where, S is the average strain rate; k is the turbulent kinetic energy; ε is the dissipation rate; μ is the dynamic viscosity caused by diffusion; μ_t is the turbulent viscosity coefficient; G_k represents the turbulent kinetic energy generated by the average velocity gradient; G_b denotes the turbulent kinetic energy generated by buoyancy; Y_M represents the influence of turbulent pulsation expansion on the total dissipation rate; $C_1=\max\left[0.43,\eta/(\eta+5)\right]$, $\eta=Sk/\varepsilon$ is a symbol, and $C_{1\varepsilon}$ is a constant; σ_k and σ_ε are the turbulent Prandtl numbers of the kinetic energy k and the dissipation rate ε, respectively; $C_{1\varepsilon}=1.44$, $C_2=1.9$, $\sigma_k=1.0$ and $\sigma_\varepsilon=1.2$ are default constants in the software.

The semi-implicit method for the pressure-linked equation (SIMPLE) algorithm was considered to solve the pressure-velocity coupling problem. The Volume of Fluid (VOF) approach was applied to capture the free surface of the two-phase flow involving water and air.

The volume of fluid (VOF) method, presented by Hirt and Nichols[18], was developed to simulate the air-water interaction, assuming that all phases in each control volume share velocity, pressure and other field functions. The High-Resolution Interface Capturing (HRIC) scheme is adopted to mimic the convective transport of immiscible fluid components, and this scheme is suited for tracking sharp interfaces.

2.2 Computational domain and boundary conditions

The computational domain plays an important role in the simulation of the flow around the tunneled planing hull, whose size has a significant influence on the accuracy and computational cost[14]. In the current study, only half of the hull was modeled due to the symmetry of the geometry. Moreover, the downstream domain of the tunneled planing hull was considered $4.0L$[1]. And the appropriate computational domain is adopted and presented in Fig.3. As can be seen, the

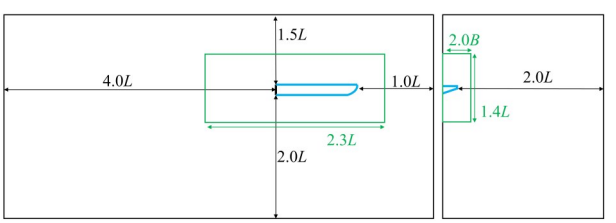

Fig.3 Main dimensions of the computational domain

background domain can be approximated as a rectangle with dimensions of 6.0L×2.0L×3.5L. And the overset domain was set as 2.3L×2.0B×1.4L.

Details of boundary conditions in this study are defined and presented in Tab.2 and Fig.4. The inlet, top, bottom and side boundaries were considered as velocity inlet which is a uniform velocity equivalent to ship speed. Hydrostatic pressure distribution was defined at the outlet boundary. The center plane of the domain was set as a symmetry condition. The tunneled planing hull was defined as a wall with no-slip condition. The interface boundaries between the background domain and overset domain were assigned the overset boundary condition and a linear interpolation technique was used to transform the information from each other region[10]. A reference coordinate system is defined by O-XYZ, which is fixed on the intersection of transom stern and keel of the hull. The positive X direction is towards the bow and the positive Y direction is towards the portside.

Tab.2 Boundary conditions

Boundary	Condition
Tunneled planing hull	Wall
Inlet	Velocity inlet
Outlet	Pressure outlet
Top	Velocity inlet
Bottom	Velocity inlet
Side	Velocity inlet
Symmetry	Symmetry
Overset	Overset mesh

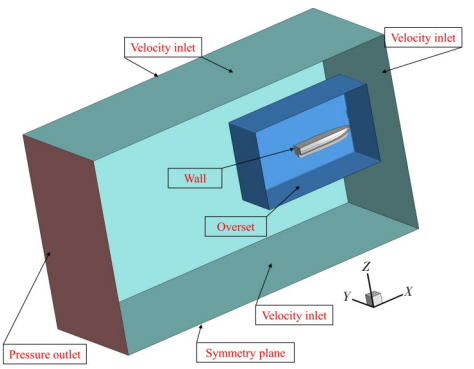

Fig.4 Schematic diagram of the boundary conditions

2.3 Mesh generation

The volume mesh of the computational domain was generated automatically by Star CCM+. The mesh of the free surface was refined to capture the wake wave and reduce the ventilation problem (see Fig.5). Volumetric controls were used to refine the mesh around the hull and free surface region in Fig.6. The prism layer mesh model was used to generate orthogonal prismatic cells next to wall boundaries, which was necessary to improve the accuracy of the flow solution around the tunneled planing hull. The trimmed cell mesh was considered to produce high-quality mesh for complex geometry problems.

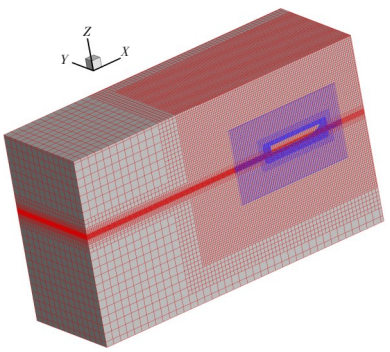

Fig.5 Overall computational mesh

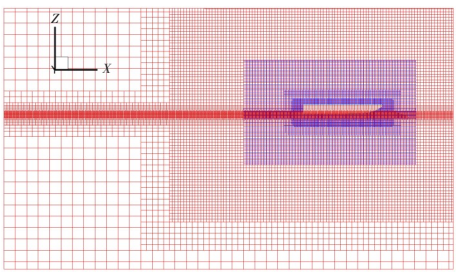

Fig.6 Refined mesh of free surface region and hull region

In this study, two-layer all y^+ treatment model is used to deal with boundary layer mesh. All y^+ wall treatment is widely used and considered for all the simulations. It is a hybrid approach that attempts to emulate the high y^+ wall treatment for coarse meshes (for $y^+ > 30$) and the low y^+ wall treatment for fine meshes (for $y^+ \approx 1$). All y^+ wall treatment can balance the computational time and proper quality of the boundary layer description[19]. Fig.7 shows the comparison of the y^+ distribution on the bottom obtained by Realizable $k-\varepsilon$ turbulence model and SST $k-\omega$ turbulence model. It can be seen that different turbulent models have a certain influence on y^+ distribution.

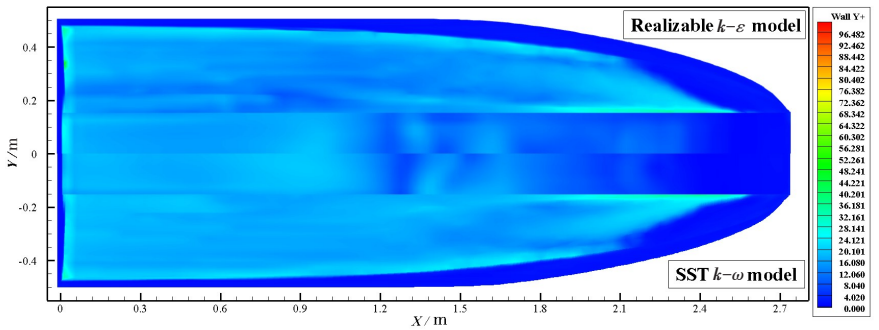

Fig.7 Comparison of y^+ distribution obtained by two different turbulent models at Fn=1.013

3 Validation

3.1 Convergence test

For CFD simulation, the numerical solution highly depends on the computational mesh and time step. To ensure the convergence of simulation, the uncertainty of grid and time step was investigated in simulation with SST $k-\omega$ turbulence model. Three sets of computational meshes with different grid numbers and three sets of simulations with different time steps at Fn=1.013 (M=159.5 kg) generated are shown in Tab.3.

Tab.3 Comparison of different meshes and time steps

Variables	No	Case	Number of meshes	Time step /s
Mesh	1	Coarse	1 360 000	0.005
	2	Medium	1 560 000	0.005
	3	Fine	1 700 000	0.005
Time step	4	Coarse	1 560 000	0.007
	5	Medium	1 560 000	0.005
	6	Fine	1 560 000	0.003

The results of CFD simulation under three different sets of meshes are summarized in Tab.4. Three time-steps for coarse (0.007 s), medium (0.005 s), and fine (0.003 s) were selected to study the convergence of the time step, as shown in Tab.5. The mesh convergence ratio obtained from the solution of the resistance for different meshes is −0.823, demonstrating the oscillatory convergence of the mesh. The convergence ratios of resistance, sinkage and trim by the different time steps are 0.438, 0.409, and 0.536, which are in the range of 0 to 1, implying that the monotonic convergence is satisfied. Considering the limitations of the computational resources, the medium grid and medium time step are adopted in the current numerical simulations to reduce the computational cost.

Tab.4 Results of mesh convergence

Mesh	Resistance /N	Error (%)	Sinkage /m	Error (%)	Trim /°	Error (%)
EFD	266.7339	–	0.0403	–	4.51	–
Coarse	244.0485	8.50	0.0472	17.07	3.25	28.02
Medium	249.7999	6.35	0.0450	11.73	3.76	16.54
Fine	245.0681	8.12	0.0443	9.99	3.81	15.57

Tab.5 Results of time step convergence

Time step	Resistance /N	Error (%)	Sinkage /m	Error (%)	Trim /°	Error (%)
EFD	266.7339	–	0.0403	–	4.51	–
Coarse	262.1518	1.72	0.0479	18.97	3.97	12.02
Medium	249.7999	6.35	0.0450	11.73	3.76	16.54
Fine	244.3922	8.38	0.0438	8.78	3.65	18.96

3.2 Resistance performance

For validation, the results of resistance, sinkage and trim angle obtained by CFD method with two different turbulent models were compared with the available experiments (M=159.5 kg). And the comparisons are presented in Figs.8–10. It can be seen clearly that the resistance of both CFD results is in good agreement with the experimental data in the range of Fn≤1.521. A certain deviation between the numerical results and experiments occurs when Fn≥1.773. The resistance obtained by SST $k-\omega$ turbulence model seems closer to the measured data than that of Realizable k–ε turbulence model, especially at high speeds.

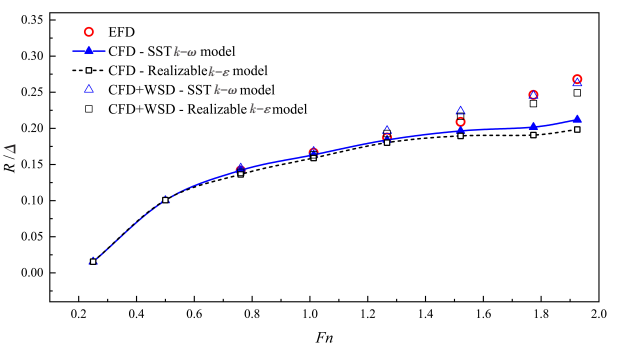

Fig.8 Comparison of numerical and experimental resistance

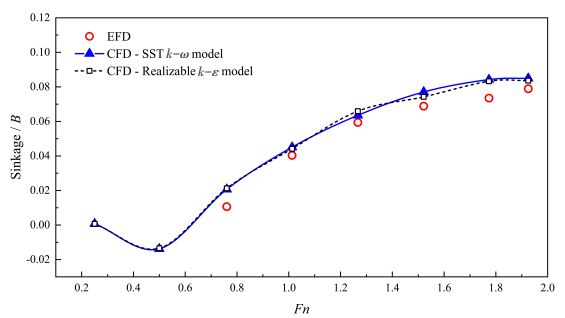

Fig.9 Results of sinkage versus Froude number

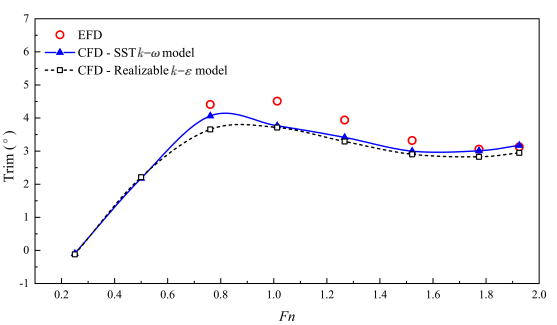

Fig.10 Results of trim angle versus Froude number

The spray resistance can constitute over 15% of the total resistance at high-speed planing regions[20]. However, the spray of flow cannot be accurately captured by the conventional numerical simulation and VOF method, which causes the deviation of numerical resistance[3, 21]. In this study, the whisker spray drag (WSD) is computed by Savitsky's equations[20] and further added to the resistance obtained by the CFD simulation. It can be seen from Fig.8 that the CFD results incorporated with the whisker spray drag(WSD) remarkably improve the accuracy of numerical resistance.

The sinkage and trim angle simulated by CFD results are in good accordance with the experimental results, which indicates that the viscous numerical simulation performed in the present

study can obtain accurate values. The numerical solution in this study can be implemented for a comprehensive investigation of the characteristics of the tunneled planing hull.

4 Results and discussion

4.1 Pressure distribution

To ensure the condition of the top of the tunnel (wet or dry) and investigate the internal flow of the tunnel, the comparison of tunnel profile, wave cut and pressure distribution along the center line at different speeds (M=159.5 kg) are plotted in Fig. 11. The position of the tunnel changes with speed due to the motion of the hull. As can be seen, the wave cut and tunnel profile have a certain distance at all speeds. This phenomenon proves that the top of the tunnel is not wetted. Due to the complete ventilation in the tunnel region, the tunnel can be considered to be a plane on an air cushion. The air flows out from the astern in the tunnel and there is an obvious ventilation phenomenon at all the speeds, which is different from the behaviors of a planing trimaran[3]. For a planing trimaran, the air flow in the tunnel is disordered and has no obvious ventilation at the early planing state[3]. In this condition, the hydrodynamic lift is negligible,whereas the aerodynamic forces become dominant in tunnel lift[15]. In the range of Fn = 0.50−1.521, the difference between the tunnel profile and the wave cut, from the bow to the stern direction, gradually decreases from the maximum value to a stable value. At the X position corresponding to the beginning of the stable value, the maximum pressure of wave cut occurs, which is caused by the extrusion of the mixed area of air and water.

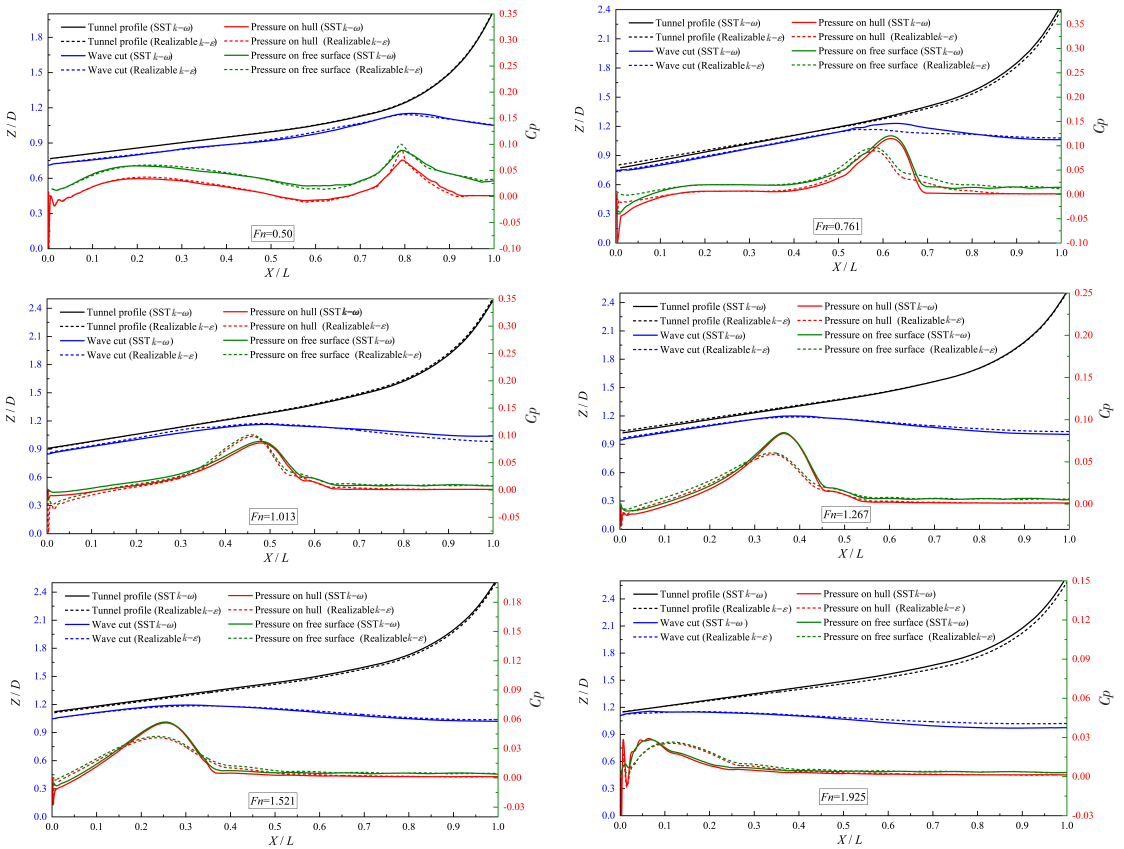

Fig.11 Comparison of pressure distributions and wave cuts longitudinally

As the speed increases, the positions of pressure peak on the hull and the wave cut gradually move astern. This is because the starting position where the tunnel and the wave cut are closest to move backward. The pressure peaks acting on the wave cut and the hull are the same at high speeds. This phenomenon indicates that when the tunneled planing hull is advancing at high speed, air entering from the tunnel of the bow and the water flowing in the tunnel forms an air-water mixture. When the tunnel is in a mixed area of air and water, the aerodynamic pressure in the tunnel has a certain relationship with the wave characteristics. With the speed increases, the air and water flow in the tunnel is completely ventilated, there is a constant difference between the pressure on the tunnel and the pressure on the wave surface (except for the peak value).

Although the peak pressure on the tunnel computed by two turbulent models has a discrepancy, the tunnel profile keeps in good agreement. This behavior implies that the difference in aerodynamic pressure on the tunnel has a small influence on the attitude of the hull.

The contours of pressure distributions on the bottom of the tunneled planing hull obtained by two turbulent models are plotted in Fig.12. With the speed increasing, the pressure distribution of the side-bottom becomes discontinuous and two major high-pressure regions appear, which is completely different from the conventional planing monohull[10]. The pressure distribution obtained by the two different turbulent models has a certain difference when $Fn \geqslant 1.521$, the pressure distribution of Realizable $k-\varepsilon$ turbulence model becomes unsmooth. As can be seen, the peak of pressure on the tunnel moves astern with an increase in speed.

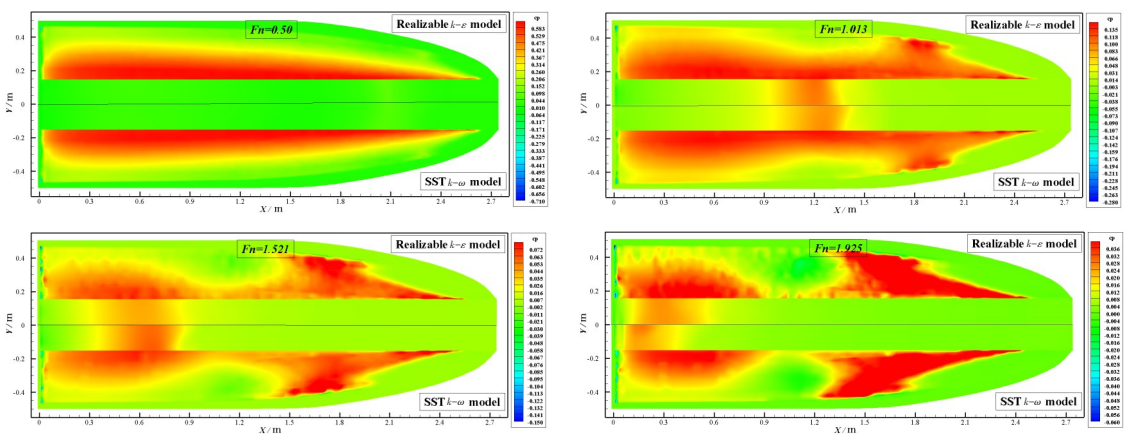

Fig.12　Contours of pressure distributions by two turbulent models

4.2 Wave profiles

The contours of the free surface obtained by the two turbulent models are shown in Fig.13. It can be observed that as the forward speed increases, the wavelength increases gradually and the angle of the 'V' shape becomes smaller. There is a hollow behind the transom stern due to the squat of the stern. The position corresponding to the bottom of the tunnel is filled with water at all speeds. This phenomenon indicates that the up of the tunnel and free surface has a certain distance, which is consistent with the behavior shown in Fig.11. The distribution of the free surface simulated by the two turbulent models shows good agreement.

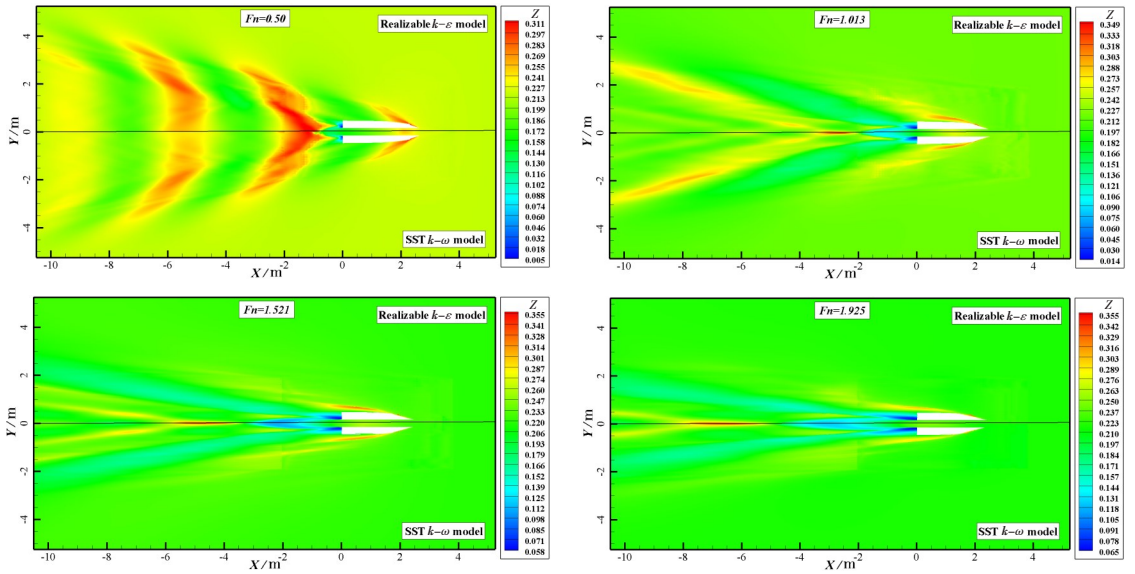

Fig.13 Contours of the free surface by two turbulent models

For further analysis, the wave cut longitudinally at three different positions is plotted in Fig.14. The wave cut of Y/L=0.076 is distributed along the side−bottom of hull. The Y/L=0.0 and Y/L=0.038 are located along the tunnel. The comparison of wave cut obtained by two models shows good agreement at all speeds. The wake profile behind the transom stern is significant for the investigation of the performance of the tunneled planing hulls[16]. As can be seen from Fig.14, the position of the peak value in the tunnel moves astern by increasing the velocity. The length of the hollow (Y/L=0.0) increases with the speed increasing, which is consistent with the previous studies[16]. It can be clearly seen that the wave cut under the tunnel (Y/L=0.0 and Y/L=0.038) is obviously different from that of Y/L=0.076.

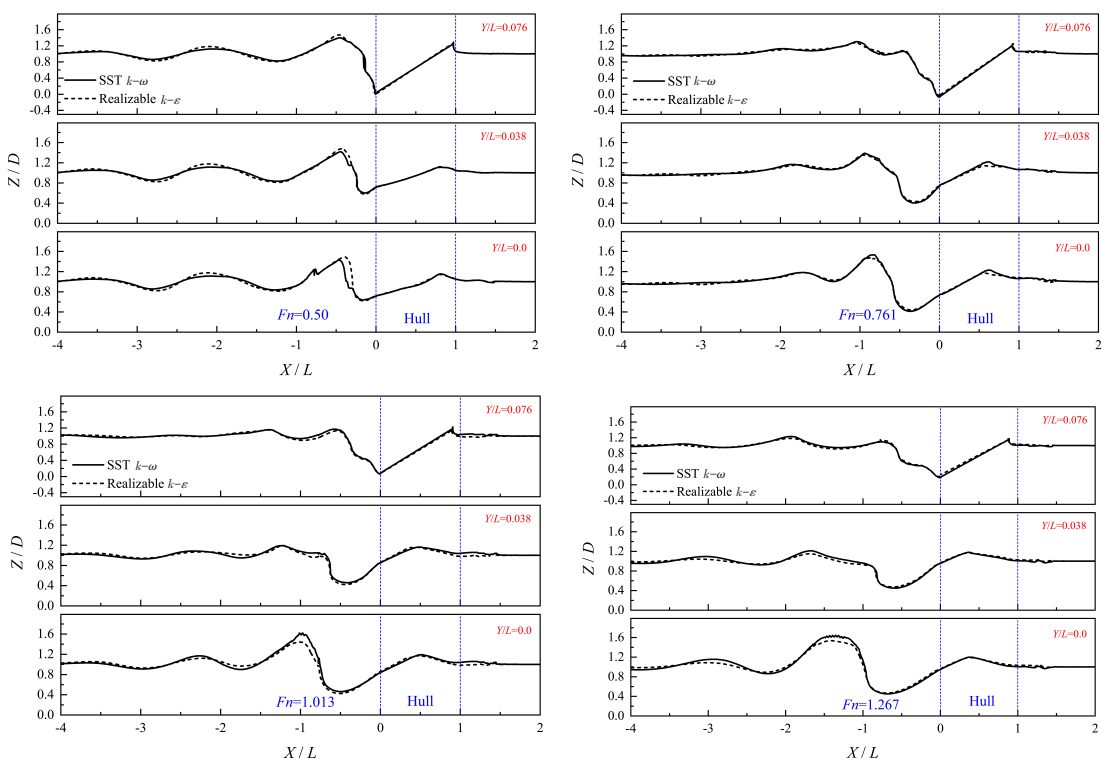

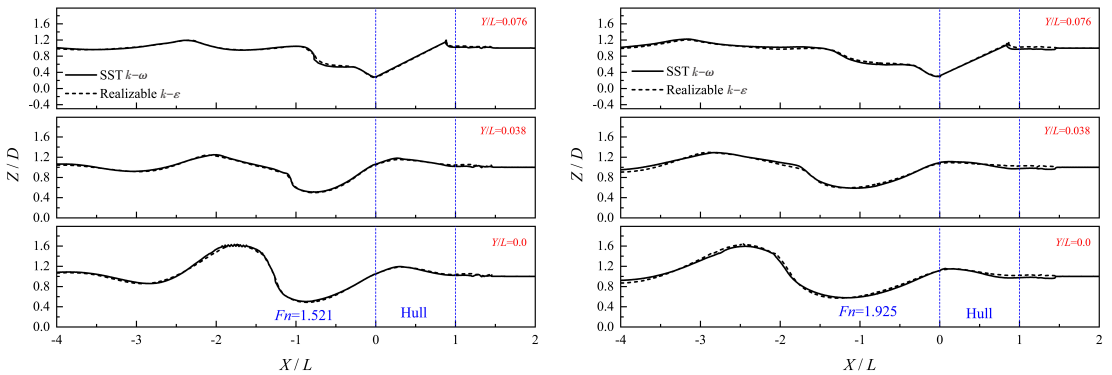

Fig.14 Wave cut longitudinally by two turbulent models

4.3 Lift force

The total lift force generated by the fluid acting on the tunneled planing hull should be equal to its gravity under steady equilibrium conditions. The total lift force (L_t) consists of the dynamic (L_d) and static lift force (L_s). The dynamic lift is the sum of the hydrodynamic lift force generated by water and the aerodynamic lift force generated by air (mainly in the tunnel). Due to the difference in density, the static lift force is almost hydrostatic lift force (or buoyancy) and the static lift force generated by air is ignored in this study.

$$L_t = L_s + L_d = Mg \tag{4}$$

where L_s denotes the static lift force and L_d represents the dynamic lift force, respectively.

The comparison of lift forces at different Froude numbers is given in Fig.15. Good agreement between the two models can be found at all the speeds. When Fn>1.267, the dynamic lift force obtained by SST $k-\omega$ turbulence model is slightly larger than that of Realizable $k-\varepsilon$ turbulence model. When Fn=0.50, the static lift force reaches up to the maximum value and the sinkage makes its minimum value. In this case, the underwater volumes of the tunneled planing hull become maximum. The static lift force exceeds 100% of the required total lift force and the dynamic lift force goes below zero where the hull experiences squat[6]. With the increase of speed, the dynamic lift force becomes positive, which implies that dynamic lift force makes a real contribution of the total lift after Fn≥0.60. When 0.60<Fn≤1.267, the static lift force is a major component of the total lift. After Fn>1.267, the dynamic lift force has achieved a dominant position in the total lift force and exceeds 50%.

The volume fraction of air of streamline around the hull at Fn=1.013 obtained by SST $k-\omega$ turbulence model is displayed in Fig.16. As can be seen from Fig.16, the complex flow occurs near the spray region and separation of water. A mixed vortex flow of the air and water is generated near the entrance of the tunnel. The air streamlines above the deck detach from the hull continuously and are twisted toward astern[9]. Khazaee et al[9] divided the local flow pattern around the prismatic planing hull into three portions. In this study, the behaviors of

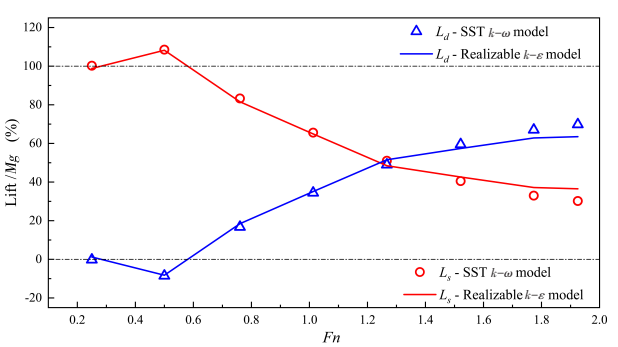

Fig.15 Comparison of lift forces at different Froude numbers

the local fluid flow near the tunneled planing hull (see Fig.16) can be divided into four regions due to the presence of the tunnel.

(a) The air streamlines located above the deck of a tunneled planing hull, which detaches from the deck.

(b) The water flow under the side-bottom and behind the transom stern.

(c) The air flow above the free surface, which can be defined three parts according to the position. The first part separates from the spray zone and breaks away from the sides. The second part separates from the bow and continues to the transom with a twisting form. The last part flows along the side of the hull and leaves the hull at the transom stern.

(d) The group of air streams under the tunnel of the hull, which can support the aerodynamic lift force and reduce the frictional resistance.

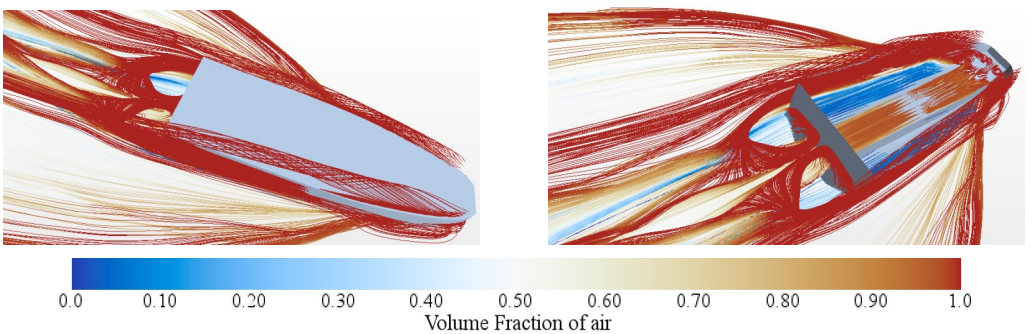

Fig.16 Volume fraction of streamline at Fn=1.013

The volume fraction of streamlines at different speeds simulated by SST k-ω turbulence model is displayed in Fig.17. It can be found that the effect of speed on the wake flow of the streamlines is obvious. With the speed increasing, the position where the air streams separated from the hull near the spray region move astern and then keep steady. The wake flow behind the transom stern becomes more complex with the speed increasing.

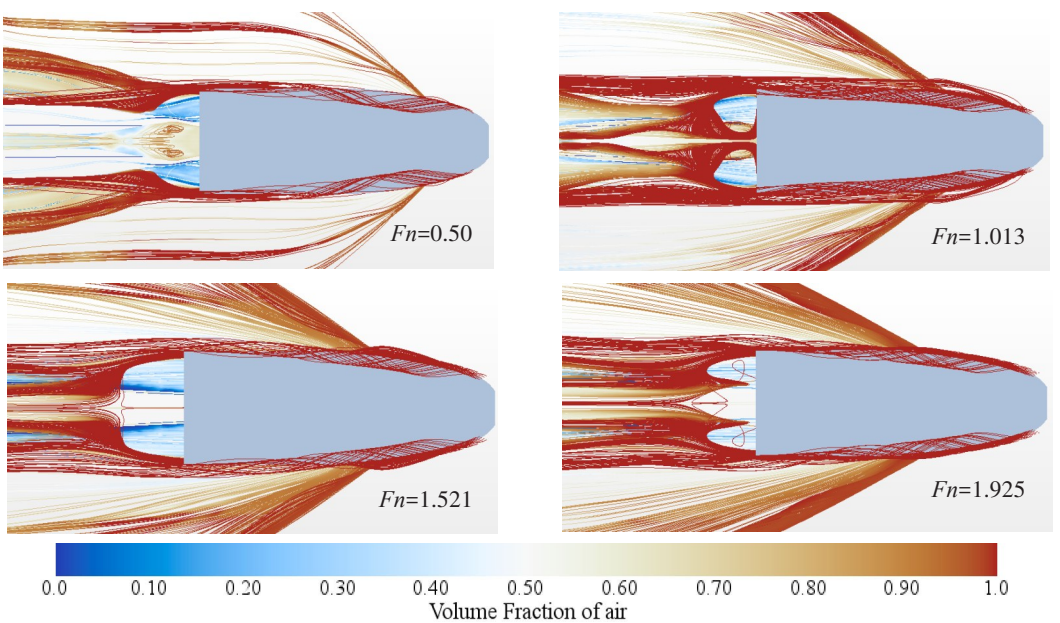

Fig.17 Volume fraction of streamlines at different speeds

5 Conclusions

In the present study, combined experimental tests and numerical simulation of a tunneled planing hull in calm water were conducted to analyze the hydrodynamic characteristics at different forward speeds. The experimental results of sinkage, trim angle and resistance were measured for the 1:4 scale model with three different masses. The comparison of the three cases shows that the trim angle increases with the increment of the amount of mass in the range of $0.761 \leqslant Fn \leqslant 1.773$. The resistance to lift ratio (R/Δ) is obviously reduced with the mass of the vessel ($Fn \geqslant 1.267$) increasing, which indicates that the tunneled planing has more advantage in terms of larger displacement[11].

The same test conditions were reproduced with the numerical simulation by using two different turbulent models, i.e. SST $k-\omega$ and Realizable $k-\varepsilon$ turbulence models. The results of numerical simulation were validated by comparison with the experimental data (M=159.5 kg). Comparison of the sinkage and trim angle obtained by numerical CFD simulation with those of experiments show good agreement.The comparison of resistance implies that the SST $k-\omega$ turbulence model can give closer results to the experiments in comparison with Realizable $k-\varepsilon$ turbulence model, especially at high speeds.

The air enters the tunnel region from the bow and flows out from the astern at all speeds. There is complete ventilation in the tunnel region, the tunnel of the hull can be considered to advance on the air cushion at all the speeds, which is distinguished from characteristics of the planing trimaran[3, 15]. With the speed increasing, the positions of the pressure peak acting on the tunnel and the wave cut along the center line in the tunnel gradually move astern. There are two major high-pressure regions on the bottom at high speed ($Fn \geqslant 1.521$), which is completely different from the conventional planing hull with a prismatic form[10].The results of pressure acting on the side-bottom of the hull obtained by the two turbulent models show good satisfaction at all the speeds, which implies that there is no significant difference between SST $k-\omega$ and Realizable $k-\varepsilon$ turbulence models for numerical simulation of high-speed planing hulls[16, 22]. The local flow around the tunneled planing hull has another portion, air streams under the tunnel of the hull due to the presence of tunnel, compared with the conventional planing monohull[9]. The tunnel flow of the tunneled planing hull and its effects on the hydrodynamic performance are complicated and required futher investigation, there is still work on the analysis of tunneled planing hull in future studies.

References

[1] Ashkezari A Z, Moradi M. Three-dimensional simulation and evaluation of the hydrodynamic effects of stern wedges on the performance and stability of high-speed planing monohull craft[J]. Appl. Ocean Res., 2021, 110: 102585.

[2] Bakhtiari M, Veysi S, Ghassemi H. Numerical modeling of the stepped planing hull in calm water[J]. Int. J. Eng. Trans. B Appl., 2016, 29: 236-245.

[3] Ding J, Jiang J. Tunnel flow of a planing trimaran and effects on resistance[J]. Ocean Eng., 2021, 237: 109458.

[4] Kim D J, Kim SY, You Y J, et al. Design of high-speed planing hulls for the improvement of resistance and seakeeping performance[J]. Int. J. Nav. Archit. Ocean Eng., 2013, 5: 161-177.

[5] Ma W, Sun H, Zou J, et al. Test research on the resistance performance of high-speed trimaran planing hull[J].Polish Mari-

time Research, 2013, 20: 45-51.
[6] Sukas O F, Kinaci O K, Cakici F, et al. Hydrodynamic assessment of planing hulls using overset grids[J]. Appl. Ocean Res., 2017, 65: 35-46.
[7] Dashtimanesh A, Esfandiari A, Mancini S. Performance prediction of two-stepped planing hulls using morphing mesh approach[J]. J. Sh. Prod. Des., 2017, 34: 236-248.
[8] Dumortier C, Bonnet J F, Regnier N, Ousten Y. Comparing results of a power prediction tool with measured data from a series of 35 boats[J]. Ocean Eng., 2019, 178: 501-516.
[9] Khazaee R, Rahmansetayesh M A, Hajizadeh S. Hydrodynamic evaluation of a planing hull in calm water using RANS and Savitsky's method[J]. Ocean Eng., 2019, 187: 106-221.
[10] Wang H, Zhu R., Huang S, Zha L. Hydrodynamic analysis of a planing hull in calm water using overset mesh and rigid body motion method[C]//Proceedings of the International Offshore and Polar Engineering Conference, Shanghai, China, 2020.
[11] Su Y M, Wang S, Shen H L, et al. Numerical and experimental analyses of hydrodynamic performance of a channel type planing trimaran[J]. S. J. Hydro Dyn., 2014, 26: 549-557.
[12] Yousefi R, Shafaghat R, Shakeri M. Hydrodynamic analysis techniques for high-speed planing hulls[J]. Appl. Ocean Res., 2013, 42: 105-113.
[13] Ghassabzadeh M, Ghassemi H. Determining of the hydrodynamic forces on the multi-hull tunnel vessel in steady motion[J]. J Braz. Soc. Mech. Sci. Eng., 2014, 36: 697-708.
[14] Jiang Y, Sun H, Zou J, et al. Analysis of tunnel hydrodynamic characteristics for planing trimaran by model tests and numerical simulations[J]. Ocean Eng. 2016, 113: 101-110.
[15] Jiang Y, Sun H B, Zou J, et al. Experimental and numerical investigations on hydrodynamic and aerodynamic characteristics of the tunnel of planing trimaran[J]. Appl. Ocean Res., 2017, 63: 1-10.
[16] Roshan F, Dashtimanesh A, Bilandi R N. Hydrodynamic characteristics of tunneled planing hulls in calm water[J]. Brodogradnja., 2020, 71: 19-38.
[17] Lee S, Paik K, Hwang H, et al. A study on ship performance in waves using a RANS solver, Part 1: Comparison of power prediction methods in regular waves[J]. Ocean Eng., 2021, 227: 108900.
[18] Hirt C W, Nichols B D. Volume of fluid (VOF) method for the dynamics of free boundaries[J]. J. Comput. Phys., 1981, 39(1): 201-225.
[19] De Marco A, Mancini S, Miranda S, et al. Experimental and numerical hydrodynamic analysis of a stepped planing hull[J]. Appl. Ocean Res., 2017, 64: 135-154.
[20] Savitsky D, Delorme M F, Datla R. Inclusion of whisker spray drag in performance prediction method for high-speed planing hulls[J]. Mar. Technol., 2007, 44: 35-56.
[21] Wang J, Zhuang J, Su Y, Bi X. Inhibition and hydrodynamic analysis of twin side-hulls on the porpoising instability of planing boats[J]. J. Mar. Sci. Eng., 2021, 9: 1-26.
[22] De Luca F, Mancini S, Miranda S, et al. An extended verification and validation study of CFD simulations for planing hulls [J]. J. Sh. Res., 2016, 60: 101-118.

槽道滑行艇水动力特性的数值研究

王 慧[1,2], 朱仁传[1], 李国焕[3], 徐德康[1], 李超凡[1]
(1. 上海交通大学 船舶海洋与建筑工程学院 海洋工程国家重点实验室, 上海 200240; 2. 武汉第二船舶设计研究所, 武汉 430205; 3. 广州船舶及海洋工程设计研究院, 广州 510250)

摘要: 由于槽道的存在,槽道滑行艇具有独特的流体动力学和空气动力学特性。本文对槽道滑行艇的水动力特性进行了试验和数值研究。在0.761≤Fn≤1.925范围内,分别进行了质量为127.4 kg、159.5 kg和202.9 kg的船模阻力试验。拖曳水池的阻力试验结果表明,排水量较大的槽道滑行艇阻力性能优越。采用基于有限体积法的雷诺平均纳维斯托克斯

(RANS)方程进行数值模拟,以分析船体在静水中具有两个自由度(升沉和纵摇)的阻力特性(M=159.5 kg)。数值结果与试验数据的比较显示出良好的一致性。比较和讨论了由SST k-ω与Realizable k-ε两种湍流模型的数值模拟获得的压力分布、波形和升力。由于槽道的存在,船体周围流线的局部流体流动可以分为四个区域,这与传统的棱柱型滑行艇的表现不同。

关键词: 槽道滑行艇; 模型试验; 重叠网格方法; 压力分布; 升力

中图分类号: U661.31　　**文献标识码**: A

基金项目: 国家自然科学基金联合基金项目"叶企孙"科学基金(U2141228)

作者简介: 王　慧(1994-),男,博士研究生;

朱仁传(1969-),男,博士生导师,上海交通大学教授;

李国焕(1992-),男,硕士;

徐德康(1996-),男,博士研究生;

李超凡(1996-),男,博士研究生。